

Experimental validation of transmutation products calculations in neutron irradiated tungsten

V. Chatzikos^{1,2,*}, M.I. Savva¹, T. Vasilopoulou¹, I.E. Stamatelatos¹, D. Terentyev³,
A. Stankovskiy³, N. Patronis² and K. Mergia¹

¹ National Centre for Scientific Research “Demokritos”, Institute of Nuclear and Radiological Science and Technology, Energy and Safety, 15341 Agia Paraskevi, Athens, Greece

² Department of Physics, University of Ioannina, Ioannina, 45110, Greece

³ SCK CEN, Boeretang 200, B-2400 Mol, Belgium

Abstract

Neutron irradiation can significantly alter the elemental composition of a material by generating transmutation products through nuclear reactions between neutrons and atomic nuclei. These changes in composition can substantially impact the material's physical and mechanical properties. Therefore, accurately assessing the buildup of transmutation products in neutron-irradiated materials is essential for understanding and predicting these effects. Tungsten (W) is particularly critical for the first wall and divertor components in fusion reactors. As such, an accurate assessment of transmutation products in neutron-irradiated tungsten is crucial for the safety and lifespan of future fusion power plants. The scope of the present work is to experimentally validate calculations of transmutation products buildup in tungsten after neutron irradiation at the Materials Test Reactor (MTR) BR-2 at SCK CEN, Belgium. Tungsten specimens were irradiated to doses of 0.12 and 0.19 displacements per atom (dpa) within the temperature range of 600 to 1200°C. Nuclide inventory calculations were performed using the FISPACT-II code and the TENDL-2019 cross-section library. γ -ray spectroscopy was employed to determine the specific activity levels of ^{181}W , ^{185}W , ^{188}W , ^{188}Re and ^{182}Ta in order to validate the transmutation products calculations for rhenium (Re), osmium (Os) and tantalum (Ta). It is shown that the theoretical calculations for Re and Os concentrations are in good agreement with the experimental data, while the Ta concentration is underestimated by a factor of approximately 1.5.

Keywords: Tungsten, neutron irradiation, transmutation products, γ -ray spectroscopy, radionuclide inventory calculations

*Corresponding Author: V. Chatzikos, v.chatzikos@ipta.demokritos.gr

1 Introduction

Tungsten (W) is a promising armor material for the divertor and the first wall in future fusion reactors, due to its numerous advantageous properties such as high melting point, high thermal conductivity, high thermal shock resistance, low coefficient of thermal expansion, high sputtering resistance, low hydrogen retention as well as low neutron activation [1–3]. The use of tungsten as a plasma facing material of the first wall and/or the divertor (heat exhaust) has been implemented in tokamak reactors, such as ASDEX Upgrade and JET [4,5]. W has also been selected for the plasma facing components of ITER [6], a fusion device that constitutes an important milestone in the roadmap towards the realization of fusion energy as a sustainable and safe energy source.

During fusion reactor operation, plasma facing components will be subject to high fast neutron fluence of energy up to 14 MeV, as well as slow neutrons due to moderation and scattering of fast neutrons from the blanket and structural materials. In tungsten, this exposure to neutron irradiation will result in displacement damage within the crystal lattice, as well as the production of rhenium (Re), osmium (Os) and tantalum (Ta) isotopes through radiative capture reactions and consequent beta decays of the products [3,7–10]. Moreover, neutron irradiation of W leads to hydrogen (H) and helium (He) production as a result of (n, p) and (n, α) reactions, respectively [3]. The accumulation of the transmutation products alters the elemental composition of W and may lead to detrimental changes in its physical and mechanical properties [3,11]. It is therefore of great importance to accurately determine the concentration of the transmutation products in neutron irradiated tungsten as well as to study their evolution with time.

In the literature, there are studies concerning the accumulation of transmutation products in neutron irradiated tungsten. Nevertheless, the number of studies offering experimental validation of the theoretical calculations remains limited. Most of these studies compare their experimental data with radionuclide inventory build-up calculations using evaluated cross-section libraries for the dominant (n, γ) reactions on W [7,8,11–14]. The transmutation products build-up depends on the energy spectrum of the incident neutrons as well as the irradiation time [7,11,12].

In [8] Atom Probe Tomography (APT) measurements were carried out on highly pure W samples irradiated at the High Flux Reactor at Petten for 208 days resulting in a total neutron fluence of 1.21×10^{26} n/m² and a total irradiation dose of 1.67 dpa and the experimental data were in good agreement with FISPACT-II (version 4.1) [15] calculations for all the detected isotopes of W, Re, Os and Ta. Qian et al [16] performed FISPACT-II simulations of W neutron irradiation for EU-DEMO first wall conditions. They showed that the transmutation products concentration in W after 10 years of continuous irradiation at a total neutron fluence of $6.6 \cdot 10^{22}$ n/cm² is (2.50 \pm 0.16) at% Re, (0.93 \pm 0.07) at% Os and (0.87 \pm 0.31) at% Ta. It has to be stressed that such concentration levels of Re, Os and Ta may have a significant impact on the mechanical and physical properties of W based components in future fusion systems.

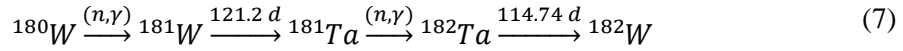
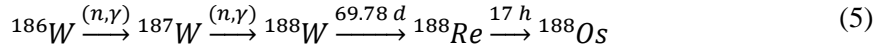
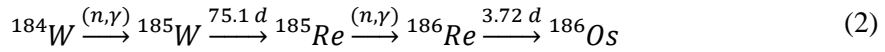
In another investigation performed by Abernethy et al. [17], γ -ray spectroscopy and energy dispersive X-ray spectroscopy was performed on single crystals of commercially pure W samples. The resultant transmutation product data was compared with FISPACT-II calculations, employing the TENDL-2017 nuclear data library [18] and a satisfactory agreement was observed.

The scope of the present work is to experimentally validate calculations of transmutation product buildup in tungsten after neutron irradiation at the Materials Test Reactor (MTR) BR-2 at SCK CEN, Belgium. Radionuclide inventory calculations were performed using the FISPACT-II code and the TENDL-2019 cross-section library [19]. The predicted specific activities of radioactive isotopes of tungsten (W),

rhodium (Rh), and tantalum (Ta) were compared against the respective values determined by γ -ray spectroscopy measurements for the irradiation doses of 0.12 and 0.19 dpa.

2 Neutron reactions in tungsten

Natural occurring tungsten consists of five isotopes: ^{180}W , ^{182}W , ^{183}W , ^{184}W and ^{186}W with atomic abundances of 0.12%, 26.5%, 14.31%, 30.64% and 28.43% respectively. The main transmutations taking place under fission neutron irradiation of tungsten are described by the nuclear reactions (1) to (7).



The reactions (1) to (7) are chosen to emphasize the radioactive isotopes that remain detectable during γ -ray spectroscopy measurements conducted at approximately 500 days post the end of neutron irradiation. Consequently, reactions leading to the creation of short-lived isotopes are omitted from this examination.

From the isotopes produced in reactions (1) to (7):

- ^{185}Re , ^{187}Re , ^{186}Os , ^{188}Os , ^{181}Ta and ^{182}W are stable isotopes and cannot be detected by γ -ray spectroscopy.
- ^{186}Re , ^{187}W and ^{188}Re produced from reaction (4) have half-lives of 3.7, 1 and 0.7 days respectively and, therefore, they have decayed at the time of the γ -ray measurements.
- ^{185}W , ^{181}W , ^{188}W , ^{182}Ta and ^{188}Re (the latter produced from reaction (5) can be detected by γ -ray spectroscopy, since they emit γ rays and have sufficiently long half-lives.

It is noted that ^{188}Re ($T_{1/2} = 17$ h) produced by reaction (5) is in transient equilibrium with ^{188}W ($T_{1/2} = 69.78$ d) which means that the activity of the daughter isotope (^{188}Re) will be almost equal to the activity of the parent isotope (^{188}W) at all times.

Notwithstanding the current study refers to neutron irradiations performed in a fission reactor, it is noted that the fission neutron spectrum is considered as adequately representative to the one encountered in the DEMO divertor. In the divertor the neutrons have already been moderated [20] and the impact of (n, 2n)

reactions on the production of radioactive isotopes of W is limited. Therefore, the main isotope production mechanism is via neutron capture reactions justifying the irradiation performed in a fission spectrum.

3 Experimental

3.1 Materials and irradiation

Three types of W materials were studied: a) high purity (99.999%) single crystal (SC) W, b) ITER grade W of 36×36 mm² cross section, forged/hammered from the two orthogonal directions (>99.97% purity), and c) “cold” rolled sheet of 1 mm thickness (>99.97% purity). The sample type will be indexed as SC, bar, or sheet respectively from now on. The SC samples were supplied by MaTeck while the bar [21] and sheet [22] samples were produced by PLANSEE SE using a powder metallurgical route consisting of sintering and forging or rolling. The W samples are disc-shaped, having a diameter of 12 mm and a thickness of 0.5 mm approximately. The chemical composition of the polycrystalline materials, as provided by PLANSEE SE, is shown in Table 1.

Table 1: Guaranteed and typical chemical composition of the polycrystalline W samples provided by PLANSEE SE.

Element	Concentration (µg/g)		Element	Concentration (µg/g)		Element	Concentration (µg/g)	
	Guaranteed	Typical		Guaranteed	Typical		Guaranteed	Typical
Ag	10	< 5	K	10	5	Zn	5	< 2
Al	15	5	Mg	5	< 2	Zr	5	< 2
As	5	< 2	Mn	5	< 2	C	30	10
Ba	5	< 2	Mo	100	20	H	5	2
Ca	5	< 2	Na	10	< 2	N	5	< 2
Cd	5	< 2	Nb	10	< 5	O	20	5
Co	10	< 2	Ni	5	< 2	P	20	< 10
Cr	20	< 5	Pb	5	< 2	S	5	< 2
Cu	10	< 5	Ta	20	< 10	Si	20	5
Fe	30	10	Ti	5	< 2			

Neutron irradiations were performed at the Materials Test Reactor (MTR) BR2 at SCK CEN, Mol, Belgium. In order to maximize the fast-to-thermal neutron ratio and thus achieve transmutation rates of W into Re and Os closer to those expected under ITER and DEMO conditions, the irradiations were performed inside a fuel element and in the maximum fast neutron flux positions (> 0.1 MeV, 7×10^{14} n/cm²/s). A top view of the BR2 reactor core configuration for cycle 05/2017 is shown in Figure 1. The red arrow indicates the irradiation channel that was used for the irradiation of the W samples investigated in this work.

3.2 γ -ray Spectroscopy

The γ -ray spectroscopy measurements were performed using a system based on a High Purity Germanium (HPGe) detector of 40% relative efficiency and energy resolution of 0.93 keV and 1.90 keV for photon energy of 122 keV and 1332 keV, respectively. The W samples were positioned at a distance of 100 cm from the detector. Preliminary measurements of the most active samples showed that the loss of counts due to the detector dead time was below 5% at that distance. Moreover, true coincidence summing was assumed to be negligible. Also, at the distance of 100 cm the disc shaped samples can be regarded as a point-source in order to further simplify the analysis. The samples were measured approximately 500 days post irradiation and the spectrum analysis was performed using the GammaVision™ software.

A typical γ -spectrum showing the most distinctive peaks of the detected isotopes is presented in Figure 2. The criteria for selecting the peaks used for the analysis were to obtain counting statistics relative uncertainty lower than 5% as well as no interference from other isotopes. The analysis of the γ -ray spectra led to the identification of five radionuclides (

Table 2) that meet those criteria and are used for the specific activity calculations, namely ^{181}W , ^{185}W , ^{188}W , ^{188}Re and ^{182}Ta .

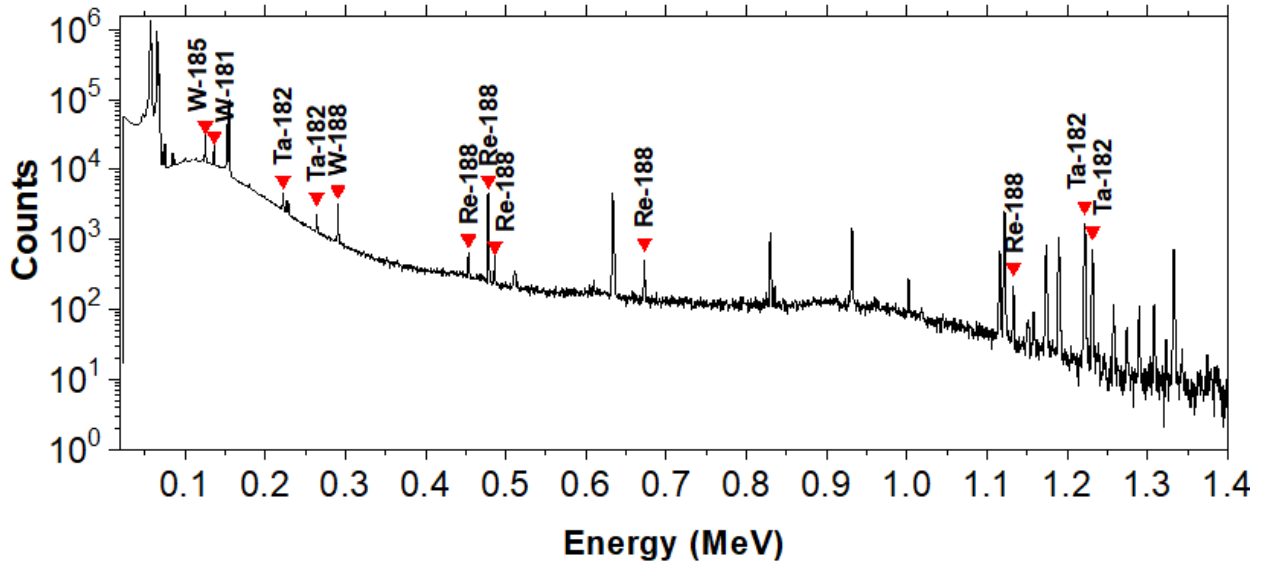


Figure 2: Representative γ - spectrum of a tungsten sample, acquired in 10800 s (3 h).

Table 2: Radionuclides, their half-lives, photon energy and emission probability for the peaks used for the γ -spectra analysis (source: <https://www-nds.iaea.org/relnsd/vcharthtml/VChartHTML.html>)

Isotope	Half-life (d)	Energy (keV)	Emission Probability (%)
^{181}W	121.2	136.28	0.03
^{185}W	75.10	125.36	0.02
^{188}W	69.78	290.68	0.416
^{188}Re	0.71	478.00	1.08
		672.54	0.12
		1132.31	0.09
		486.09	0.08
		453.34	0.07
^{182}Ta	114.74	1221.40	27.23
		1231.00	11.62
		222.11	7.57
		264.07	3.61

For the isotopes in which more than one peak is detected, the averaged specific activity is calculated based on a weighted average of the activities, where the weights are determined by the uncertainties associated with the net areas of the selected peaks. This approach follows the methodology described by Gilmore [27]. Correction factors were applied to account for the attenuation of the emitted photons by the samples themselves as well as by a Plexiglass sample-holder used in the measurements. The main factors contributing to the uncertainty of the experimental results are the statistical uncertainty of the counting and the uncertainty in the detection efficiency. Both factors result in relative uncertainties reaching up to 5%.

4 Calculations

Theoretical calculation of the transmutation product activities was performed using the nuclide inventory code FISPACT-II and cross-section data from the TENDL-2019 (709 energy groups) library. The neutron spectrum and fluence required for these calculations were assessed by SCK CEN detailed MCNP 6.1 model of the BR-2 reactor core including the irradiation channels. The MCNP 6.1 calculations were extended to estimate the effects of neutron self-shielding from the samples and neutron attenuation from the materials of the capsule.

4.1 Neutron fluence estimation

Monte Carlo simulations were performed using the Monte Carlo code MCNP (version 6.1) [28]. The simulations were performed in two stages. First, the neutron energy spectrum was calculated at the axial position of the irradiation capsule for an empty channel. Then, simulations were performed to take into consideration neutron shielding from the irradiation capsule and the samples. A spherical neutron source was assumed with energy spectrum as calculated by SCK CEN for the empty channel. The source emits neutrons isotropically (uniform emission in all directions), while the irradiation capsule and samples

were modeled in detail at its center. A drawing of the irradiation capsule containing the W samples and the geometry used for the MCNP 6.1 calculations are depicted in Figure 3.

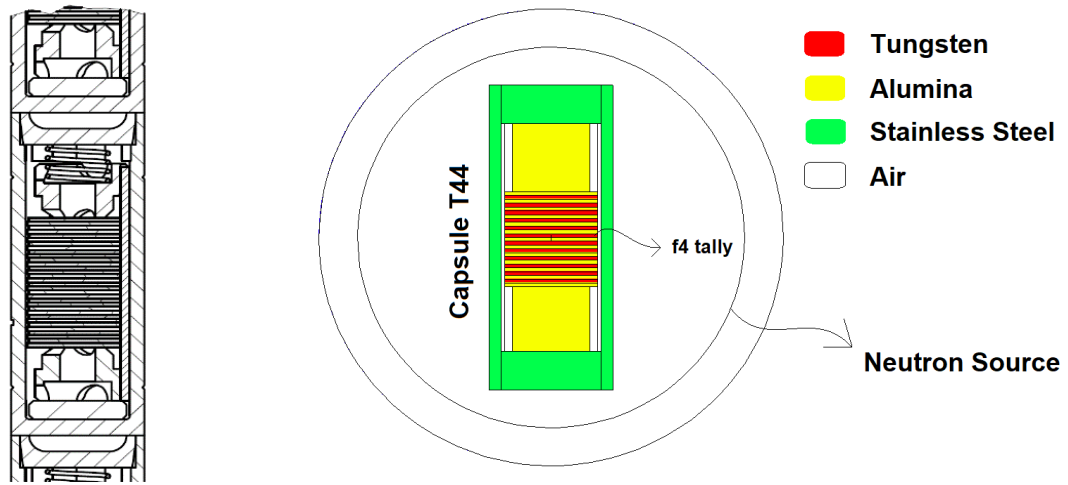


Figure 3: a) Detailed drawing of the irradiation capsule including the W samples b) MCNP 6.1 geometry simulating the irradiation capsule.

The simulations were performed using the ENDF/B-VII.1 [29] cross section library. A specialized track length neutron fluence tally was precisely positioned to record the incident neutron spectrum at the location of the irradiated material. The calculated spectra were used as input for the subsequent FISPACT-II calculations. The predicted neutron spectrum at the middle of the irradiation channel is shown in Figure 4. The neutron flux uncertainty was 10%.

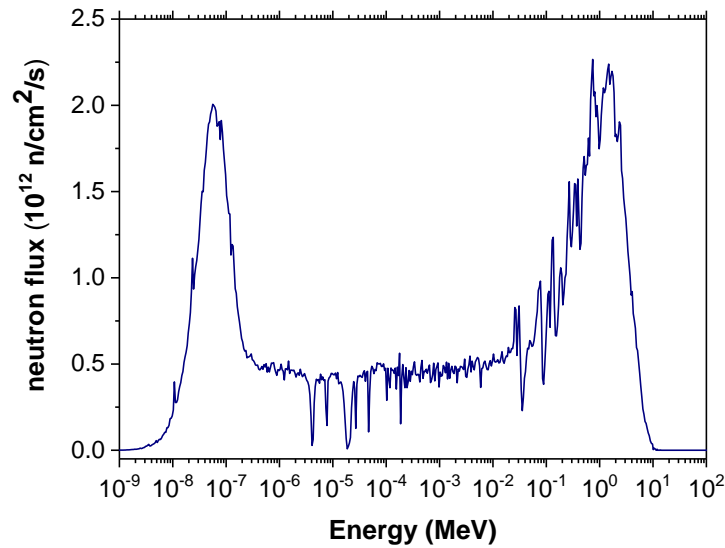


Figure 4: Predicted neutron spectrum at the middle of the irradiation channel.

4.2 Nuclide inventory calculations

The transmutation products in the neutron irradiated tungsten samples were calculated using the FISPACT-II nuclide inventory code. Input parameters were the isotopic composition of the sample, the energy dependent cross-sections, as well as the predicted incident neutron spectrum determined as described above. The MCNP 6.1 calculated neutron spectra at each irradiation position were applied to predict the transmutation products in 1 g of pure natural W. The natural isotopes of W were used as the target nuclides for the FISPACT-II calculations and the exact irradiation cycle times were considered. The transmutation product concentrations as well as the specific activities of the radioactive isotopes of W, Re and Ta were calculated for the date that the γ -ray spectroscopy measurements were completed (500 d after the end of irradiation). According to the calculations, the transmutation product concentrations have reached over 99% (96% for Ta) of their saturation values at the time of the measurements. FISPACT-II calculations using both TENDL-2019 and ENDF/B-VII.1 regarding transmutation product concentrations gave similar results within the uncertainty interval, at a confidence level of 95%.

5 Results

5.1 Pathway analysis

Pathway analysis was performed in order to determine the most abundant transmutation product isotopes and the major reaction chains that lead to their production. The product isotopes, the reaction chain and at% contribution in the production of the isotope, as well as their abundance in the produced element is shown in Table 3 for both irradiation doses.

Table 3: Target and product nuclides, reaction chain and its contribution as well as the isotopic abundance of the most important isotopes of Re, Os and Ta calculated by FISPACT-II using the TENDL-2019 cross section library for the doses of 0.12 and 0.19 dpa.

Product Element	Target Nuclide	Reaction Chain	Reaction contribution (at %)		Product Nuclide	Product Nuclide Abundance (at %)	
			0.12 dpa	0.19 dpa		0.12 dpa	0.19 dpa
Rhenium	^{184}W	(1)	100		^{185}Re	8	
	^{186}W	(3)	100		^{187}Re	92	
Osmium	^{184}W	(2)	100		^{186}Os	4	8
	^{186}W	(4)	86.5	90	^{188}Os	96	92
		(5)	13.5	10			
Tantalum	^{180}W	(6)	100		^{181}Ta	100	

As shown in

Table 3, ^{188}Re , ^{188}Os and ^{181}Ta constitute approximately 92%, 92-96% and 100% of the produced Rhenium, Osmium and Tantalum respectively, while reactions (3), (4) and (6) are dominant in the production of those isotopes. It is noted that as the irradiation dose increases, the contribution of reaction (4) to the total ^{188}Os production increases. For example, for the dose of 0.19 dpa the contribution to the total ^{188}Os production increases from 86.5% to 90% while the ^{188}Os contribution to the total Os concentration decreases from 96% to 92% since more ^{186}Os is produced.

5.2 Transmutation products

The FISPACT-II calculated transmutation product concentrations for 1 g tungsten samples irradiated at 0.12 and 0.19 are shown in Table 4 and Table 5 respectively, for the different axial positions in the irradiation rig. It is noted that different axial positions in the rig correspond to different sample irradiation temperatures. It is also stressed that MCNP simulations for the determination of the neutron spectrum in the center of the empty irradiation channel were performed using temperature corrected cross-section data. However, calculations for the second stage to determine the neutron spectra in the presence of the samples and the holder showed no statistically meaningful discrepancies for different irradiation temperatures.

Table 4: Transmutation product concentrations of the 0.12 dpa samples (fast neutron fluence 5.8×10^{20} n/cm², >0.1 MeV) calculated with FISPACT-II inventory code using the TENDL-2019 cross section library.

Axial position (mm)	Irradiation temperature (°C)	Re (at%)	Os (10^{-2} at %)	Ta (10^{-3} at%)
-30	1200	0.42±0.05	0.8±0.2	1.7±0.2
10	900	0.41±0.04	0.7±0.2	1.6±0.2
50	800	0.39±0.04	0.7±0.1	1.6±0.2
90	600	0.38±0.04	0.6±0.1	1.5±0.2
Average		0.40±0.04	0.7±0.2	1.6±0.2

Table 5: Transmutation product concentration of the 0.19 dpa samples (fast neutron fluence 8.9×10^{20} n/cm², >0.1 MeV) calculated with FISPACT-II inventory code using the TENDL-2019 cross section library.

Axial position (mm)	Irradiation temperature (°C)	Re (at%)	Os (10^{-2} at%)	Ta (10^{-3} at%)
-70	1200	0.59±0.07	1.5±0.3	2.4±0.3
-110	900	0.57±0.06	1.5±0.3	2.4±0.3
-150	800	0.56±0.06	1.4±0.3	2.3±0.3
-190	600	0.54±0.06	1.3±0.3	2.3±0.3
Average		0.57±0.06	1.4±0.3	2.4±0.3

The uncertainties reported in Table 4 and Table 5 include the uncertainty in the incident neutron flux, which is the main component, as well as the cross-section and lifetime uncertainties. The concentrations of all the transmutation products are higher towards the center of the irradiation rig, since the neutron flux presents its maximum value at the center of the irradiation channel.

5.3 γ -ray spectroscopy

The specific activity derived from the γ -ray spectroscopy experimental data is compared against FISPACT-II calculations using the TENDL-2019 nuclear data library in Figure 5 to Figure 8. The uncertainty that arises in the specific activities calculated with FISPACT-II is a combination of the cross section and half-life uncertainties, with the cross-section uncertainty being the dominant contributor at all cases. Both experimental data and FISPACT-II calculation results refer to the same date, which is approximately 500 days after the irradiation end. The data pertaining to the ^{188}Re isotope have been excluded since this isotope is in a transient equilibrium with ^{188}W , rendering the resulting graphs identical.

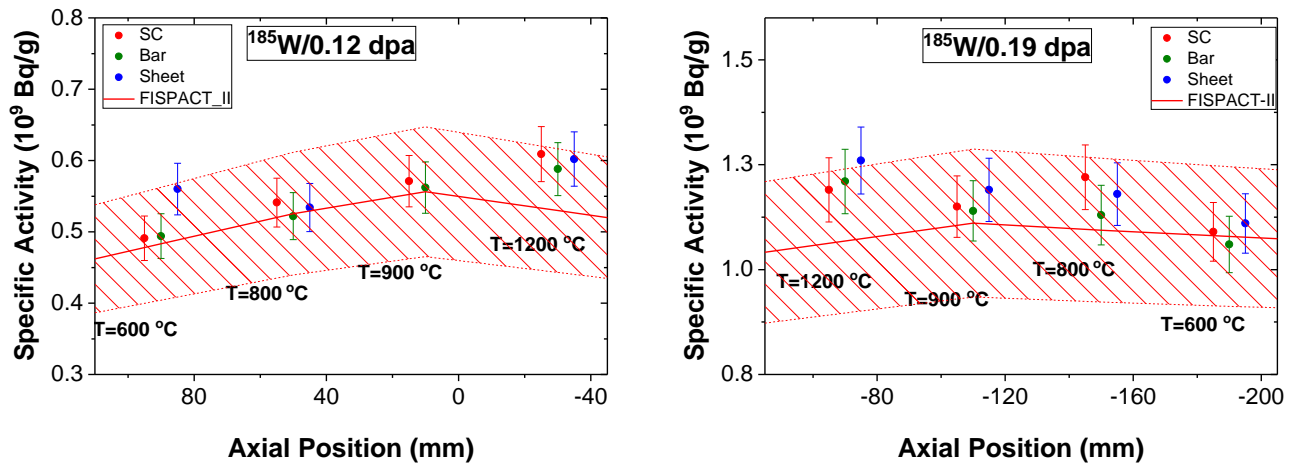


Figure 5: Specific activity of ^{185}W for 0.12 and 0.19 dpa samples approximately 500 d post irradiation compared to FISPACT-II calculations using TENDL-2019.

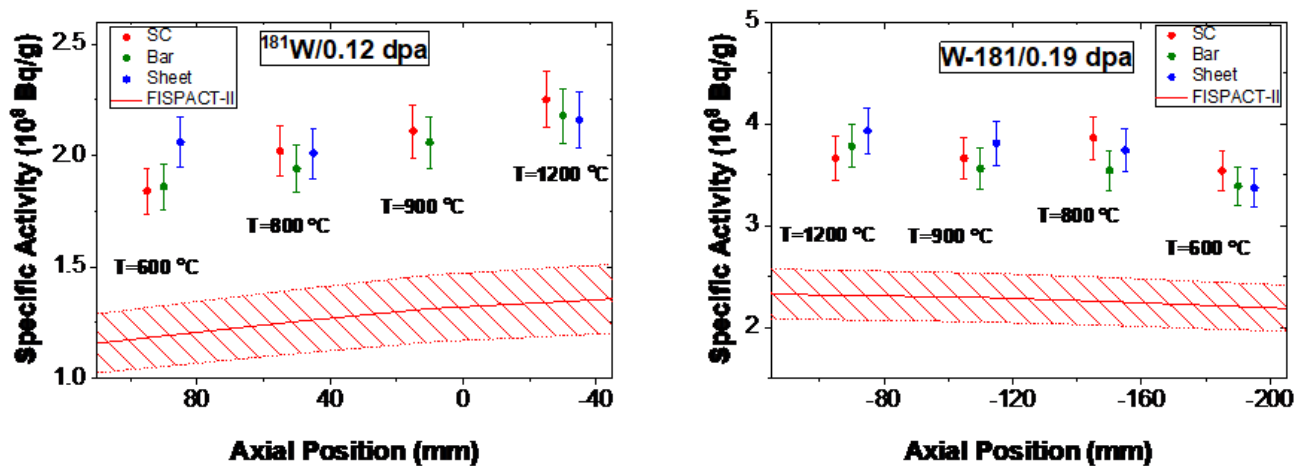


Figure 6: Specific activity of ^{181}W for 0.12 and 0.19 dpa samples approximately 500 d post irradiation compared to FISPACT-II calculations using TENDL-2019.

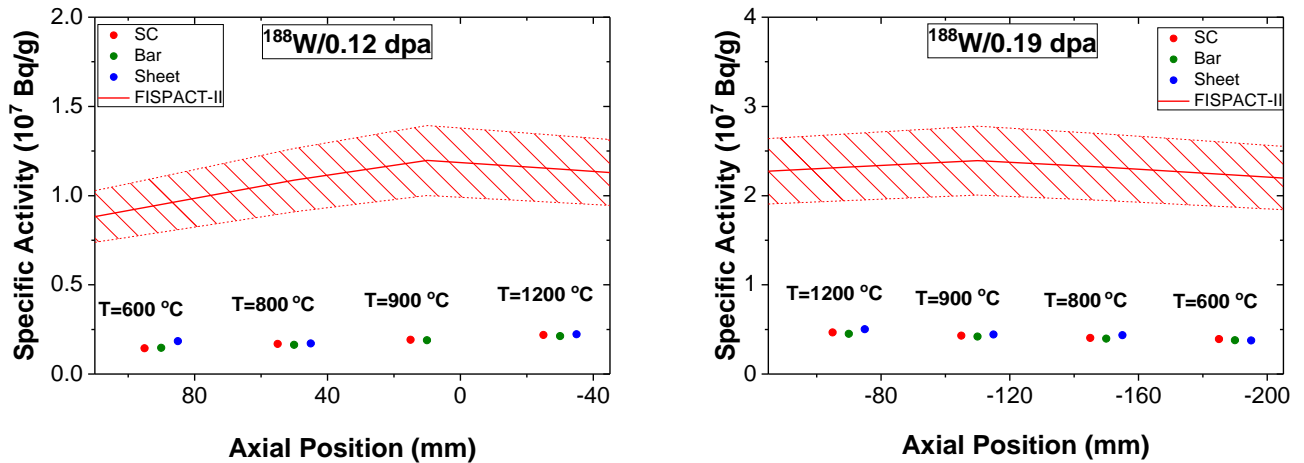


Figure 7: Specific activity of ^{188}W for 0.12 and 0.19 dpa samples approximately 500 d post irradiation compared to FISPACT-II calculations using TENDL-2019.

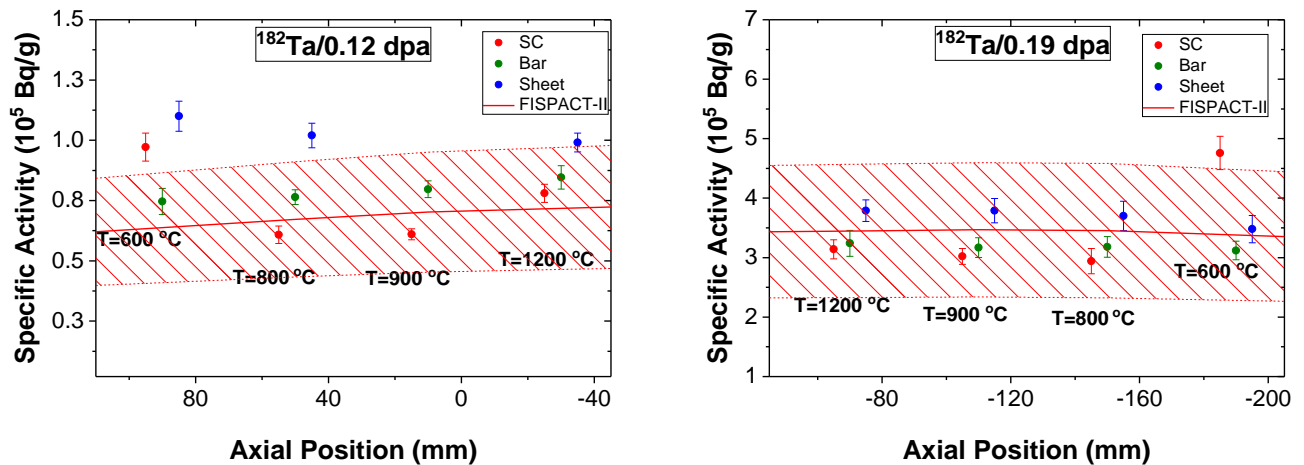


Figure 8: Specific activity of ^{182}Ta for 0.12 and 0.19 dpa samples approximately 500 d post irradiation compared to FISPACT-II calculations using TENDL-2019.

The ^{185}W specific activity values (Figure 5) calculated using the FISPACT-II inventory code is in good agreement with the experimental results. As shown in

Table 3, this agreement provides confidence for the 8% of the total rhenium production, since ^{185}Re is produced from ^{185}W through reaction (1).

Regarding ^{181}W , the calculated specific activity values (

Figure 6) are lower than the corresponding experimental data by a factor of 1.5. Since ^{181}W disintegrates into ^{181}Ta , it may be concluded that the calculations underestimate the total Ta concentration produced by ^{181}W by a factor of approximately 1.5, as well.

In the case of ^{188}W , which impacts the production of ^{188}Re , the average calculated specific activity is about 4.5 times higher than the corresponding experimental value (Figure 9).

As far as ^{182}Ta is concerned, the calculated specific activity (Figure 8) values are in good agreement with the experimental data. Nevertheless, since ^{182}Ta disintegrates to ^{182}W (reaction (7)) which is a stable isotope of tungsten, this reaction does not affect the transmutation production.

Discrepancies are observed for the various axial positions, which are attributed to the neutron flux variation along the irradiation channel (Figure 5 - Figure 8). Nevertheless, the total neutron fluence was found not to significantly change between samples of the same irradiation dose. The calculated variation in fluence was of 4-5% per capsule for the 0.12 dpa samples and 2-3% per capsule for the 0.19 dpa samples.

Focusing on the transmutation production of the W samples after the neutron irradiation, FISPACT-II calculations using the TENDL-2019 cross section library resulted in (0.40 ± 0.04) at% Re, $(0.7\pm 0.2)\times 10^{-2}$ at% Os and $(1.6\pm 0.2)\times 10^{-3}$ at% Ta on average (for the four axial positions) for the irradiation dose of 0.12 dpa. The concentrations increase to (0.57 ± 0.06) at% Re, $(1.4\pm 0.3)\times 10^{-2}$ at% Os and $(2.4\pm 0.3)\times 10^{-3}$ at% Ta on average for the irradiation dose of 0.19 dpa.

6 Discussion

In the following section, the results of the experimental and calculated specific activities comparison are being discussed with respect to the observed discrepancies.

A satisfactory agreement was observed between the theoretical and experimental specific activity of ^{185}W which is responsible for the production of 8% of total rhenium the ^{185}Re isotope. However, in the case of ^{181}W , lower calculated specific activity values, by a factor of ~ 1.5 , were obtained as compared to the experimental data. Since the concentration of ^{181}W is related to the total tantalum concentration in the sample, it is concluded that Ta concentration is underestimated. The observed discrepancy is attributed to inaccuracies of the cross-section data from the TENDL-2019 library. It is noted that calculations performed using the EAF-2010 [30] cross section library resulted in agreement with the experimental data for ^{181}W . Given the ^{180}W low abundance of 0.12% in natural W, a precise measurement of the thermal neutron-capture cross section is challenging and consequently there is considerable variation of almost a factor of two amongst the published experimental data. The reported values in the literature are (20.5 ± 4.2) b [31], (22.6 ± 1.7) b [32], 30^{+120}_{-30} b [33] and (37.3 ± 2.4) b [34]. The corresponding thermal cross section for EAF-2010 is 37.4 b [30] and for TENDL-2019 is 22.3 b [19].

Regarding the substantial discrepancy, approximately by a factor of ~ 4.5 , found for ^{188}W (and consequently ^{188}Re) one has to take into account the following. The available experimental cross section data present high discrepancies, since it is difficult to experimentally measure the radiative capture neutron cross section in ^{187}W due to its short half-life of 23.72 h [35]. Gillette in 1965 [36] determined the thermal neutron (σ_0) and resonance integral (I_0) cross sections as 64 b and 2760 b, respectively. Ersöz et al. [35] reported considerably lower thermal neutron and resonance integral cross sections of (6.5 ± 0.8) b and (280 ± 35) b, respectively. Moreover, large-scale production yields of ^{188}W at the ORNL High Flux Isotope Reactor were found to be lower than theoretical yields by almost one order of magnitude [37,38]. This substantial deviation in the measured neutron cross section of ^{187}W , being of one order of magnitude lower than the values in the TENDL-2019 library ($\sigma_0=65.998$ b and $I_0=1573.77$ b), may offer an explanation for the observed discrepancy between calculated and experimental ^{188}W specific activity values. Nevertheless, the uncertainty in the $^{187}\text{W}(n, g)^{188}\text{W}$ reaction cross section is anticipated to have small impact on the transmutation product results since reaction chain (5) contributes approximately 10% to the total Osmium production (Table 3).

The specific activity values of ^{182}Ta calculated using the TENDL-2019 cross section library are in good agreement with the experimental data. The concentration of ^{182}Ta does not affect the transmutation products, it is used however as an indication of the initial tantalum impurity levels amongst the tungsten materials (highest in sheet, lowest in SC material).

It is noted that the TENDL-2019 cross section library was produced using evaluated data based on the nuclear model code TALYS [18]. The TALYS data are generated based on the nuclei properties and by either default or adjusted parameters of nuclear models across a wide collection of isotopic evaluations. This means that the data in the entire collection have been tested in detail for many isotopes against

individual experimental data, while for other isotopes such as ^{181}W and ^{187}W is as good as the global quality of TALYS.

Therefore, the results of this study demonstrate the need for a re-evaluation of the $^{180}\text{W}(n,\gamma)^{181}\text{W}$ and $^{187}\text{W}(n,\gamma)^{188}\text{W}$ reaction cross section on the basis on new experimental data. This will not only give a new perspective for the scientific community as to these reactions but also improve the nuclear data for technological and research uses.

7 Summary and Conclusions

In this study, SC, bar and sheet tungsten samples were irradiated at the BR2 research reactor at doses of 0.12 and 0.19 displacements per atom (dpa) at the temperature of 600, 800, 900 and 1200° C. The specific activity of five radioactive isotopes (^{181}W , ^{185}W , ^{188}W , ^{188}Re and ^{182}Ta) was measured using γ -ray spectroscopy and the data was compared to theoretical calculations using the FISPACT-II inventory code and the TENDL-2019 cross section library. Neutronic transport simulations were also carried out using the MCNP 6.1 code, in order to calculate the incident neutron spectrum at each irradiation position while taking into consideration phenomena such as neutron attenuation by the irradiation capsule and neutron shielding by the sample itself. The MCNP calculated neutron spectra were used as an input for the FISPACT-II calculations.

The theoretical calculations using the TENDL-2019 cross section library result in (0.40 ± 0.04) at% Re, $(0.7\pm 0.2)\times 10^{-2}$ at% Os and $(1.6\pm 0.2)\times 10^{-3}$ at% Ta on average for the irradiation dose of 0.12 dpa, which increases to (0.57 ± 0.06) at% Re, $(1.4\pm 0.3)\times 10^{-2}$ at% Os and $(2.4\pm 0.3)\times 10^{-3}$ at% Ta on average for the irradiation dose of 0.19 dpa.

The results on the transmutation product concentrations were validated by the comparison of the calculated specific activity values with the corresponding experimental data for each detected radioisotope. This comparison showed a good agreement in the cases of ^{185}W and ^{182}Ta , while notable discrepancies were observed in the cases of ^{181}W and ^{188}W (and consequently ^{188}Re).

In the case of ^{181}W , the calculated specific activities were 1.5 times lower than the corresponding experimental data. According to the calculations, ^{181}Ta , the decay product of ^{181}W , accounts for 100% of the total produced Ta. A larger discrepancy was observed for ^{188}W , where the theoretical values were approximately 4.5 times higher than the experimental data. This discrepancy is attributed to the cross-section values of the $^{187}\text{W} \xrightarrow{(n,\gamma)} ^{188}\text{W}$ reaction due to the difficulties in measuring this radiative capture neutron cross section, owing to the short half-life of the ^{187}W isotope. However, this reaction has a small effect on the total Osmium production of about 10%.

Lastly, the calculated specific activity values of ^{182}Ta are consistent with the experimental results. However, the ^{182}Ta concentration does not affect the transmutation products, but it is an indication of the initial tantalum impurities within the tungsten materials.

Based on the analysis performed in this study, it was concluded that the theoretical calculations performed with FISPACT-II and the TENDL-2019 cross section library describe adequately the Re and Os concentrations while they result in reduced Ta concentration values by a factor of approximately 1.5.

Acknowledgements

This work has been carried out within the framework of the EUROfusion Consortium, funded by the European Union via the Euratom Research and Training Programme (Grant Agreement Nos 633053 and 101052200 — EUROfusion). Views and opinions expressed are however those of the author(s) only and do not necessarily reflect those of the European Union or the European Commission. Neither the European Union nor the European Commission can be held responsible for them. The funding from the Hellenic General Secretariat for Research and Innovation for the Greek National Programme of the Controlled Thermonuclear Fusion is acknowledged. Also is acknowledged the support of the programme “NCSR – INRASTES research activities in the framework of the national RIS3” (MIS 5002559) which is implemented under the “Action for the Strategic Development on the Research and Technological Sector”, funded by the Operational Programme "Competitiveness, Entrepreneurship and Innovation" (NSRF 2014-2020) and co-financed by Greece and the European Union (European Regional Development Fund).

We thank Dr Michael Rieth from Karlsruhe Institute of Technology, Germany, and Dr Gerald Pintsuk from Forschungszentrum Jülich GmbH, Germany, for the supply of the tungsten “cold” rolled sheet and forged bar material, respectively.

References

- [1] S. Wurster, N. Baluc, M. Battabyal, T. Crosby, J. Du, C. García-Rosales, A. Hasegawa, A. Hoffmann, A. Kimura, H. Kurishita, R.J. Kurtz, H. Li, S. Noh, J. Reiser, J. Riesch, M. Rieth, W. Setyawan, M. Walter, J.-H. You, R. Pippan, Recent progress in R&D on tungsten alloys for divertor structural and plasma facing materials, *Journal of Nuclear Materials* 442 (2013) S181–S189. <https://doi.org/10.1016/j.jnucmat.2013.02.074>.
- [2] G. Pintsuk, Tungsten as a Plasma-Facing Material, in: *Comprehensive Nuclear Materials*, Elsevier, 2012: pp. 551–581. <https://doi.org/10.1016/B978-0-08-056033-5.00118-X>.
- [3] Q. Zhao, Z. Zhang, M. Huang, X. Ouyang, Effects of transmutation elements in tungsten, *Comput Mater Sci* 162 (2019) 133–139. <https://doi.org/10.1016/j.commatsci.2019.03.002>.
- [4] R. Neu, R. Dux, A. Kallenbach, T. Pütterich, M. Balden, J.C. Fuchs, A. Herrmann, C.F. Maggi, M. O’Mullane, R. Pugno, I. Radivojevic, V. Rohde, A.C.C. Sips, W. Suttrop, A. Whiteford, the A.U. Team, Tungsten: an option for divertor and main chamber plasma facing components in future fusion devices, *Nuclear Fusion* 45 (2005) 209–218. <https://doi.org/10.1088/0029-5515/45/3/007>.
- [5] R.G. Abernethy, Predicting the performance of tungsten in a fusion environment: a literature review, *Materials Science and Technology* 33 (2017) 388–399. <https://doi.org/10.1080/02670836.2016.1185260>.
- [6] R.A. Pitts, X. Bonnin, F. Escourbiac, H. Frerichs, J.P. Gunn, T. Hirai, A.S. Kukushkin, E. Kaveeva, M.A. Miller, D. Moulton, V. Rozhansky, I. Senichenkov, E. Sytova, O. Schmitz, P.C. Stangeby, G. De Temmerman, I. Veselova, S. Wiesen, Physics basis for the first ITER tungsten divertor, *Nuclear Materials and Energy* 20 (2019) 100696. <https://doi.org/10.1016/j.nme.2019.100696>.
- [7] L.R. Greenwood, F.A. Garner, Transmutation of MO , Re , W , Hf , and V in various irradiation test facilities and STARFIRE, *Journal of Nuclear Materials* 215 (1994) 635–639. [https://doi.org/https://doi.org/10.1016/0022-3115\(94\)90136-8](https://doi.org/https://doi.org/10.1016/0022-3115(94)90136-8).
- [8] M.J. Lloyd, R.G. Abernethy, M.R. Gilbert, I. Griffiths, P.A.J. Bagot, D. Nguyen-Manh, M.P. Moody, D.E.J. Armstrong, Decoration of voids with rhenium and osmium transmutation products in neutron irradiated single crystal tungsten, *Scr Mater* 173 (2019) 96–100. <https://doi.org/10.1016/j.scriptamat.2019.07.036>.
- [9] A. Hasegawa, M. Fukuda, S. Nogami, K. Yabuuchi, Neutron irradiation effects on tungsten materials, *Fusion Engineering and Design* 89 (2014) 1568–1572. <https://doi.org/10.1016/j.fusengdes.2014.04.035>.
- [10] M. Dürschnabel, M. Klimenkov, U. Jäntschi, M. Rieth, H.C. Schneider, D. Terentyev, New insights into microstructure of neutron-irradiated tungsten, *Sci Rep* 11 (2021) 1–17. <https://doi.org/10.1038/s41598-021-86746-6>.

- [11] M.E. Sawan, Transmutation of Tungsten in Fusion and Fission Nuclear Environments, *Fusion Science and Technology* 66 (2014) 272–277. <https://doi.org/10.13182/FST13-717>.
- [12] M.R. Gilbert, J.-Ch. Sublet, Neutron-induced transmutation effects in W and W-alloys in a fusion environment, *Nuclear Fusion* 51 (2011) 043005. <https://doi.org/10.1088/0029-5515/51/4/043005>.
- [13] M.R. Gilbert, J.-Ch. Sublet, S.L. Dudarev, Spatial heterogeneity of tungsten transmutation in a fusion device, *Nuclear Fusion* 57 (2017) 044002. <https://doi.org/10.1088/1741-4326/aa5e2e>.
- [14] C.B.A. Forty, G.J. Butterworth, J.-Ch. Sublet, Burnup of some refractory metals in a fusion neutron spectrum, *Journal of Nuclear Materials* 212–215 (1994) 640–643. [https://doi.org/10.1016/0022-3115\(94\)90137-6](https://doi.org/10.1016/0022-3115(94)90137-6).
- [15] J.-Ch. Sublet, J.W. Eastwood, J.G. Morgan, M.R. Gilbert, M. Fleming, W. Arter, FISPACT-II: An Advanced Simulation System for Activation, Transmutation and Material Modelling, *Nuclear Data Sheets* 139 (2017) 77–137. <https://doi.org/10.1016/j.nds.2017.01.002>.
- [16] Y. Qian, M.R. Gilbert, L. Dezerald, D. Cereceda, Using first-principles calculations to predict the mechanical properties of transmuting tungsten under first wall fusion power-plant conditions, *Journal of Physics Condensed Matter* 33 (2021). <https://doi.org/10.1088/1361-648X/ac08b8>.
- [17] R.G. Abernethy, J.S.K.L. Gibson, A. Giannattasio, J.D. Murphy, O. Wouters, S. Bradnam, L.W. Packer, M.R. Gilbert, M. Klimenkov, M. Rieth, H.C. Schneider, C.D. Hardie, S.G. Roberts, D.E.J. Armstrong, Effects of neutron irradiation on the brittle to ductile transition in single crystal tungsten, *Journal of Nuclear Materials* 527 (2019) 151799. <https://doi.org/10.1016/j.jnucmat.2019.151799>.
- [18] A.J. Koning, D. Rochman, Modern Nuclear Data Evaluation with the TALYS Code System, *Nuclear Data Sheets* 113 (2012) 2841–2934. <https://doi.org/10.1016/j.nds.2012.11.002>.
- [19] A.J. Koning, D. Rochman, J.-Ch. Sublet, N. Dzysiuk, M. Fleming, S. van der Marck, TENDL: Complete Nuclear Data Library for Innovative Nuclear Science and Technology, *Nuclear Data Sheets* 155 (2019) 1–55. <https://doi.org/10.1016/j.nds.2019.01.002>.
- [20] S. Breidokaite, G. Stankunas, Neutron Flux in EU DEMO Divertor Cassette Body Using HCPB and WCLL Breeding Blanket Models, *Journal of Fusion Energy* 41 (2022). <https://doi.org/10.1007/s10894-022-00327-7>.
- [21] M. Wirtz, I. Uytendhouwen, V. Barabash, F. Escourbiac, T. Hirai, J. Linke, T. Loewenhoff, S. Panayotis, G. Pintsuk, Material properties and their influence on the behaviour of tungsten as plasma facing material, *Nuclear Fusion* 57 (2017). <https://doi.org/10.1088/1741-4326/aa6938>.

- [22] S. Bonk, J. Reiser, J. Hoffmann, A. Hoffmann, Cold rolled tungsten (W) plates and foils: Evolution of the microstructure, *Int J Refract Metals Hard Mater* 60 (2016) 92–98. <https://doi.org/10.1016/j.ijrmhm.2016.06.020>.
- [23] T. Goorley, M. James, T. Booth, F. Brown, J. Bull, L.J. Cox, J. Durkee, J. Elson, M. Fensin, R.A. Forster, J. Hendricks, H.G. Hughes, R. Johns, B. Kiedrowski, R. Martz, S. Mashnik, G. McKinney, D. Pelowitz, R. Prael, J. Sweezy, L. Waters, T. Wilcox, T. Zukaitis, Initial MCNP6 Release Overview, *Nucl Technol* 180 (2012) 298–315. <https://doi.org/10.13182/NT11-135>.
- [24] D.B. Pelowitz, J.W. Durkee, J.S. Elson, M.L. Fensin, J.S. Hendricks, M.R. James, R.C. Johns, G.W. Mckinney, S.G. Mashnik, J.M. Verbeke, L.S. Waters, T.A. Wilcox, MCNPXTM User’s Manual, Version 2.7.0, Los Alamos National Laboratory, Los Alamos, 2011.
- [25] K. SHIBATA, O. IWAMOTO, T. NAKAGAWA, N. IWAMOTO, A. ICHIHARA, S. KUNIEDA, S. CHIBA, K. FURUTAKA, N. OTUKA, T. OHSAWA, T. MURATA, H. MATSUNOBU, A. ZUKERAN, S. KAMADA, J. KATAKURA, JENDL-4.0: A New Library for Nuclear Science and Engineering, *J Nucl Sci Technol* 48 (2011) 1–30. <https://doi.org/10.1080/18811248.2011.9711675>.
- [26] M.J. Norgett, M.T. Robinson, I.M. Torrens, A proposed method of calculating displacement dose rates, *Nuclear Engineering and Design* 33 (1975) 50–54. [https://doi.org/10.1016/0029-5493\(75\)90035-7](https://doi.org/10.1016/0029-5493(75)90035-7).
- [27] G.R. Gilmore, *Practical Gamma-Ray Spectrometry*, John Wiley & Sons, Ltd, Chichester, UK, 2008. <https://doi.org/10.1002/9780470861981>.
- [28] A.J. Goorley, John T.; James, Michael R.; Booth, Thomas E.; Brown, Forrest B.; Bull, Jeffrey S.; Cox, Lawrence J.; Durkee, Joe W. Jr.; Elson, Jay S.; Fensin, Michael Lorne; Forster, Robert A. III; Hendricks, John S.; Hughes, H. Grady III; Johns, Russell C.; Ki, Initial MCNP6 Release Overview - MCNP6 version 1.0 - LA-UR-13-22934, (2013) 0–42.
- [29] M.B. Chadwick, M. Herman, P. Obložinský, M.E. Dunn, Y. Danon, A.C. Kahler, D.L. Smith, B. Pritychenko, G. Arbanas, R. Arcilla, R. Brewer, D.A. Brown, R. Capote, A.D. Carlson, Y.S. Cho, H. Derrien, K. Guber, G.M. Hale, S. Hoblit, S. Holloway, T.D. Johnson, T. Kawano, B.C. Kiedrowski, H. Kim, S. Kunieda, N.M. Larson, L. Leal, J.P. Lestone, R.C. Little, E.A. McCutchan, R.E. MacFarlane, M. MacInnes, C.M. Mattoon, R.D. McKnight, S.F. Mughabghab, G.P.A. Nobre, G. Palmiotti, A. Palumbo, M.T. Pigni, V.G. Pronyaev, R.O. Sayer, A.A. Sonzogni, N.C. Summers, P. Talou, I.J. Thompson, A. Trkov, R.L. Vogt, S.C. van der Marck, A. Wallner, M.C. White, D. Wiarda, P.G. Young, ENDF/B-VII.1 nuclear data for science and technology: Cross sections, covariances, fission product yields and decay data, *Nuclear Data Sheets* 112 (2011) 2887–2996. <https://doi.org/10.1016/j.nds.2011.11.002>.
- [30] J.-C. Sublet, L.W. Packer, J. Kopecky, R.A. Forrest, A.J. Koning, D.A. Rochman, EASY Documentation Series The European Activation File: EAF-2010 neutron-induced cross section library, n.d.

- [31] A.M. Hurst, R.B. Firestone, L. Szentmiklósi, Zs. Révay, M.S. Basunia, T. Belgya, J.E. Escher, M. Krtička, N.C. Summers, B.W. Sleaford, New Measurement of the Thermal-capture Cross Section for the Minor Isotope ^{180}W , *Nuclear Data Sheets* 119 (2014) 91–93. <https://doi.org/10.1016/j.nds.2014.08.026>.
- [32] W.G. Kang, Y.D. Kim, J.I. Lee, I.S. Hahn, A.R. Kim, H.J. Kim, Measurement of the thermal neutron capture cross section of ^{180}W , *Phys Rev C* 76 (2007) 067602. <https://doi.org/10.1103/PhysRevC.76.067602>.
- [33] H. Pomerance, Thermal Neutron Capture Cross Sections, *Physical Review* 88 (1952) 412–413. <https://doi.org/10.1103/PhysRev.88.412>.
- [34] P.N. Vorona, O.I. Kalchenko, V.G. Krivenko, Experimental investigations of neutron cross-sections of tungsten isotope atomic nuclei: radioactive ^{181}W ($T_{1/2} = 121.2$ days) and stable ^{180}W , in: *The 2-Nd International Conference “Current Problems in Nuclear Physics and Atomic Energy,” Kyiv, 2008*.
- [35] O.A. Ersöz, R. Spink, J.R. Griswold, F. Yurt, S. Mirzadeh, Measurement of neutron capture cross section of ^{187}W for production of ^{188}W , *Applied Radiation and Isotopes* 148 (2019) 191–196. <https://doi.org/10.1016/j.apradiso.2019.03.039>.
- [36] J.H. Gillette, I.B. comp. Lane, REVIEW OF RADIOISOTOPES PROGRAM, 1964, Oak Ridge, TN (United States), 1965. <https://doi.org/10.2172/4602815>.
- [37] F.F. (Russ) Knapp, A.P. Callahan, A.L. Beets, S. Mirzadeh, B.T. Hsieh, Processing of reactor-produced ^{188}W for fabrication of clinical scale alumina-based $^{188}\text{W}/^{188}\text{Re}$ generators, *Applied Radiation and Isotopes* 45 (1994) 1123–1128. [https://doi.org/10.1016/0969-8043\(94\)90026-4](https://doi.org/10.1016/0969-8043(94)90026-4).
- [38] S. Mirzadeh, F.F. Knapp, A.P. Callahan, Production of Tungsten-188 and Osmium-194 in a Nuclear Reactor for New Clinical Generators, (1992) 595–597. https://doi.org/10.1007/978-3-642-58113-7_169.